Applied Physics Letters

A gas curtain beam profile monitor using beam induced fluorescence for high intensity charged particle beams

Cite as: Appl. Phys. Lett. **120**, 174101 (2022); https://doi.org/10.1063/5.0085491
Submitted: 17 January 2022 • Accepted: 06 April 2022 • Published Online: 27 April 2022

A. Salehilashkajani, H. D. Zhang, M. Ady, et al.

Applied Physics Letters ARTICLE scitation.org/journal/apl

A gas curtain beam profile monitor using beam induced fluorescence for high intensity charged particle beams

Cite as: Appl. Phys. Lett. **120**, 174101 (2022); doi: 10.1063/5.0085491
Submitted: 17 January 2022 · Accepted: 6 April 2022 ·
Published Online: 27 April 2022

A. Salehilashkajani,[1,2] H. D. Zhang,[1,2,a)] M. Ady,[3] N. Chritin,[3] P. Forck,[4] J. Glutting,[3] O. R. Jones,[3] R. Kersevan,[3] N. Kumar,[1,2] T. Lefevre,[3] T. Marriott-Dodington,[3] S. Mazzoni,[3] I. Papazoglou,[3] A. Rossi,[3] G. Schneider,[3] O. Sedlacek,[1,2,3] S. Udrea,[4] R. Veness,[3] and C. P. Welsch[1,2]

AFFILIATIONS

[1]The Cockcroft Institute, Daresbury, Warrington WA4 4AD, United Kingdom
[2]Department of Physics, University of Liverpool, Liverpool L69 3BX, United Kingdom
[3]CERN, 1211 Geneva, Switzerland
[4]GSI Helmholtzzentrum für Schwerionenforschung, 64291 Darmstadt, Germany

[a)]Author to whom correspondence should be addressed: hao.zhang@cockcroft.ac.uk

ABSTRACT

A minimally invasive transverse beam profile monitor based on supersonic gas curtain technology and beam-induced fluorescence has been developed and demonstrated. The concept presented can be used to measure both the profile of the proton beam in the Large Hadron Collider (LHC) and the concentricity of the electron and the proton beams in the LHC hollow electron lens. In this Letter, the performance of such a monitor for a low energy electron beam is discussed, which paves the way for its wider implementation.

The planned High Luminosity upgrade to the Large Hadron Collider (HL-LHC) is under way. This project aims to increase the integrated luminosity of the LHC by a factor of 10 to enable further studies of the Higgs boson and physics beyond the standard model.[1] An active halo control will be required for this upgrade due to the increased beam intensity. This can be achieved by a Hollow Electron Lens (HEL),[2–6] assuming that the proton beam and hollow electron beam can be kept well aligned in such a device. To measure the profile of the two co-propagating beams and ensure the alignment, a minimally invasive monitor is needed.

Minimally invasive methods based on the interaction between residual gas and particle beams, such as ionization profile monitors (IPM)[7–11] and beam induced fluorescence (BIF) monitors,[12–16] have been used or proposed for various machines. For BIF monitors or the recent beam-gas vertex detector in the LHC,[17] additional residual gas will often be introduced to create a pressure bump, thus increasing the signal to noise (S/N) ratio. As an alternative, a metal vapor jet[18,19] or a gas jet[20–24] can produce a controllable pressure bump more effectively and cause minimal impact on the beam and the surrounding vacuum environment.

Both residual gas and gas curtain IPMs would suffer from distortions due to space charge[25] and external electromagnetic fields in the LHC and HEL, where 1 T magnetic field is estimated at the diagnostic location. This leaves BIF monitors using a gas curtain with a short-lived ionic or a neutral emitter as the most feasible solution to measuring a two-dimensional transverse beam profile in machines, where the beams have high intensity and destructive power. For beams operated in an ultra-high vacuum (UHV) environment, a directional gas curtain developed from a cold supersonic source is preferable to a diffusive one.[26] Gas jets used in nuclear experiments[27,28] and laser wakefield accelerators[29] have undergone extensive research, development, and optimization, which broadened the choice of working gases and densities.

This Letter illustrates the working principle behind such a monitor and presents research highlights. The working principle has been applied to the design of a profile monitor that is currently being intended to be installed in the LHC and will contribute to the design of an overlap monitor integrated into the HEL.[30] Moreover, this can be applied to a wide range of accelerated beams with different vacuum environments.

This monitor relies on measuring the fluorescence due to the interaction between a particle beam and a supersonic gas curtain.

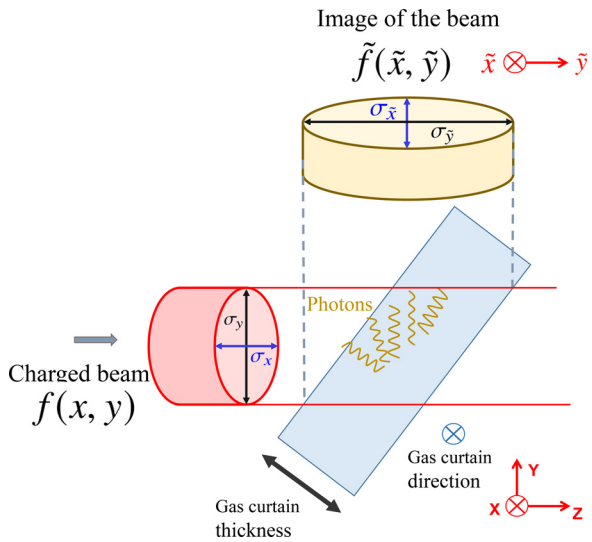

FIG. 1. The interaction point between the gas curtain and the incoming particle beam.

The gas curtain is angled at 45° and propagates perpendicularly to the beam direction as shown in Fig. 1, for two-dimensional profile detection.

The schematic of the gas curtain beam profile monitor at the Cockcroft Institute (CI) is displayed in Fig. 2. The device consists of a gas injection section, an interaction chamber, and a gas dump section. In the gas injection section, a nozzle-skimmers assembly separates the volume into three chambers. The assembly contains a nozzle with an aperture of 30 μm in diameter and two conical skimmers with diameters of 180 and 400 μm, which are aligned with an accuracy of 20 μm.[31] In the nozzle chamber, the gas with a stagnation pressure of 5 bar passes through the nozzle and experiences a free expansion to form a supersonic jet, with a smooth transition from a continuum flow region to a molecular flow region.[32] The two skimmers extract and collimate the supersonic jet. The diffusion of ambient gas molecules is suppressed via differential pumping. The third skimmer, a 0.1-mm-thick stainless steel foil with a rectangular slit of 4×0.4 mm^2 angled at 45°, shapes the gas jet into a curtain. The pressure in each chamber with and without a continuous jet flow is given in Table I. It shows the vacuum environment in the interaction chamber satisfies the requirements for most accelerators. The gas curtain's transverse density distribution is measured at the dump section using a movable pressure gauge and interpolated to the interaction point by assuming a geometrical expansion from the third skimmer which is a good approximation from the molecular flow theory. The thickness was interpolated to be approximately 0.7 ± 0.3 mm at the interaction point. The interpolated densities for the three working gases, nitrogen, argon, and neon were $(4 \pm 1) \times 10^{15}$, $(6.0 \pm 2.0) \times 10^{15}$, and $(1.4 \pm 0.4) \times 10^{16}$ m^{-3}, respectively, and the distribution is quasi-uniform with a 20% variation.[33]

TABLE I. Measured pressure (mbar) in each vacuum chamber, with gas jet off and gas jet on at a stagnation pressure of 5 bars.

Jet	Nozzle	Skimmer I	Skimmer II	Interaction	Dump
Off	5.0×10^{-8}	5.0×10^{-8}	4.0×10^{-8}	$<1.0 \times 10^{-9}$	$<1.0 \times 10^{-9}$
On	3.9×10^{-3}	8.4×10^{-6}	7.3×10^{-7}	4.0×10^{-9}	1.4×10^{-9}

A continuous electron source with 5 keV energy and 0.66 mA current was used to test this monitor. The fluorescence photons were recorded by an optical imaging system[34] placed outside the interaction chamber. The imaging system includes an apochromatic lens, a filter wheel, an intensifier, and a camera. Note that double micro-channel plates with chevron geometry were used in the intensifier to allow for spatially resolved single photon detection.[35,36] To reduce the background light due to stray photons, the interaction chamber's inner surface was covered with graphite lubricating resistance coating with a reflectivity of around 30%. In addition, for each of the gases,

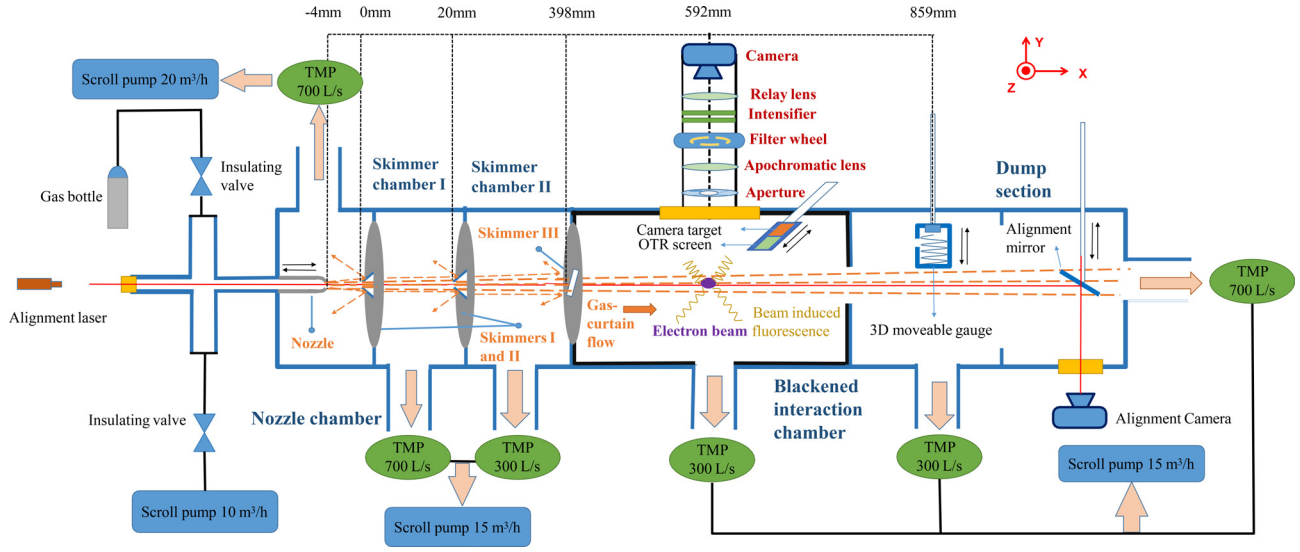

FIG. 2. The schematic diagram of the gas curtain beam profile monitor. The setup consists of six vacuum chambers, each with a dedicated turbo-molecular pump (TMP).

TABLE II. Estimated cross sections and photon rates[37] from the gas curtain for the CI electron beam (5 keV–0.66 mA), the HEL test stand electron beam (10 keV–5 A) and the LHC proton beam (7 TeV–1 A). The optical parameter is the optical acceptance multiplied by optical attenuation for each wavelength.

Emitter	Wave-length (nm)	FLT (ns)	Optical parameter	Cross-section (cm^2)			Photon rate (counts/s)		
				CI beam	HEL beam	LHC beam	CI beam	HEL beam	LHC beam
N_2^+	391.4	60	2.9×10^{-4}	1.6×10^{-18}	9.1×10^{-19}	3.7×10^{-20}	$(4.9 \pm 3.9) \times 10^{1}$	$(1.9 \pm 1.5) \times 10^{5}$	$(1.5 \pm 1.2) \times 10^{3}$
Ne	585.4	16	2.6×10^{-4}	2.7×10^{-20}	1.4×10^{-20}	4.7×10^{-22}	2.6 ± 2.2	$(8.9 \pm 7.4) \times 10^{3}$	$(6.0 \pm 5.0) \times 10^{1}$
Ar^+	476.5	16	5.6×10^{-4}	9.9×10^{-21}	5.7×10^{-21}	9.9×10^{-22}	$(8.7 \pm 6.9) \times 10^{-1}$	$(3.3 \pm 2.6) \times 10^{3}$	$(1.2 \pm 1.0) \times 10^{2}$

narrow-band filters with a 10 nm bandwidth centered at the fluorescence lines with the largest cross sections were used and placed on a filter wheel.

The fluorescence photon rate is defined as the number of photons detected by the imaging system per unit time due to the fluorescence emission from the beam/gas curtain interaction. It depends on the fluorescence cross section, the density and the thickness of the gas curtain, the current and energy of the beam, as well as the acceptance and attenuation of the optical system.[38]

The photon rate has been estimated for the electron beam at the CI, in addition to the electron beam of the HEL (5 A, 10 keV) and the proton beam of the LHC (1 A, 7 TeV) for the HL-LHC application.[37] Due to lack of data for the cross sections for the beam species and energies of interest, estimates have been calculated using extrapolations based on different theoretical models[39–41] and experimental data.[12,42–50] These estimates were then used to calculate the expected photon rates; this information is presented in Table II. For the electron beams, a factor of 2 is a realistic uncertainty on the estimated cross section. For the LHC proton beam, further verification will be required. The fluorescence life-times (FLT) for nitrogen,[12] neon, and argon[51] are also presented in Table II.

For the measurements, the photon counting method was used.[35,36] A series of frames have been taken with an exposure time of 2 s. The exposure time is chosen to ensure that all photon events in the frame, which appeared as bright spots of more than four adjacent pixels, can be individually identified. A median filter and threshold are applied to each frame to remove fake photon events, and the brightest pixel of each spot was recorded as the photon event center pixel. Photon events at each pixel are stacked over the series of frames to create an image of the beam. This way non-zero pixels will record the number of photons proportional to the beam intensity at a given location, and thus, noise from the CMOS camera is significantly reduced.

To measure the one-dimensional profile of the beam in each direction, the photons within a region of interest (ROI) are integrated horizontally and vertically and the data are smoothed using a moving average of the neighboring 15 points. For neon and argon, due to larger statistical fluctuations, 3 pixels were additionally binned together.

The gray-scale image of the electron beam obtained from the fluorescence induced in a nitrogen gas curtain is shown in Fig. 3; the ability of this monitor to produce a two-dimensional beam image is demonstrated. The background gas signal, although weak, is visible as a straight rectangular area along the $\tilde{y}$-axis. To cross-check the profile measurements using the gas curtain, the electron beam was also imaged using Optical Transition Radiation (OTR) released from an aluminum mirror connected to a linear bellows drive. The electron beam had the same energy and current for both sets of measurements; however, for the OTR measurements, the integration time was set to 320 μs and no narrow band filters were used. Furthermore, for the OTR measurements, the intensity per pixel was integrated horizontally and vertically instead of the single photon detection method since the light yield was strong enough. In Fig. 4, the two-dimensional image using both methods as well as the one-dimensional profile with a Gaussian fit are displayed. The root-mean-square (RMS) (σ_{beam}) sizes measured with both methods in the $\tilde{x}$ direction are 0.62 ± 0.02 and 0.65 ± 0.01 mm and in the $\tilde{y}$ direction are 0.88 ± 0.04 and 0.78 ± 0.01 mm for the gas curtain and the OTR, respectively. The error shown in the RMS size only includes a fitting error with 95% confidence bounds.

Multiple sources of error may affect the measured profile. Broadening of the profile in the $\tilde{y}$ direction due to the thickness of the gas curtain is one of them. Simulations of a Gaussian beam and a uniform gas curtain have shown that this broadening of profile increases with increasing thickness. In our case, given that the gas curtain thickness is on the order of one σ_{beam}, the simulations suggest the measured profile remains Gaussian with a 10% broadening ($\sigma_{measured} = 1.1\sigma_{beam}$), which is confirmed when comparing the OTR measurements and the gas curtain measurements in the $\tilde{y}$ direction. The width of the third skimmer can be reduced to minimize this broadening effect at the expense of a reduction in signal strength. The second source is the smearing of the profile due to the gas-jets thermal velocity spread. In the case of nitrogen, with an FLT of 60 ns, the longest for the three working gases studied, the distortion is approximately 8 μm considering the velocity spread of 133 m/s (at 20 K) and thus can be ignored.

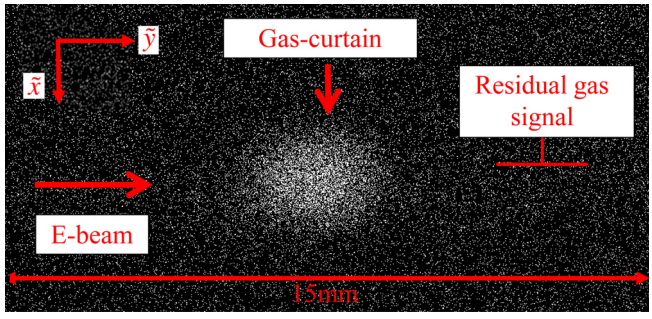

FIG. 3. A nitrogen gas curtain at a stagnation pressure of 5 bars is used to image an electron beam with a current of 0.66 mA and an energy of 5 keV. This image is compiled from 200 frames; each frame in the series has a 2 s exposure time.

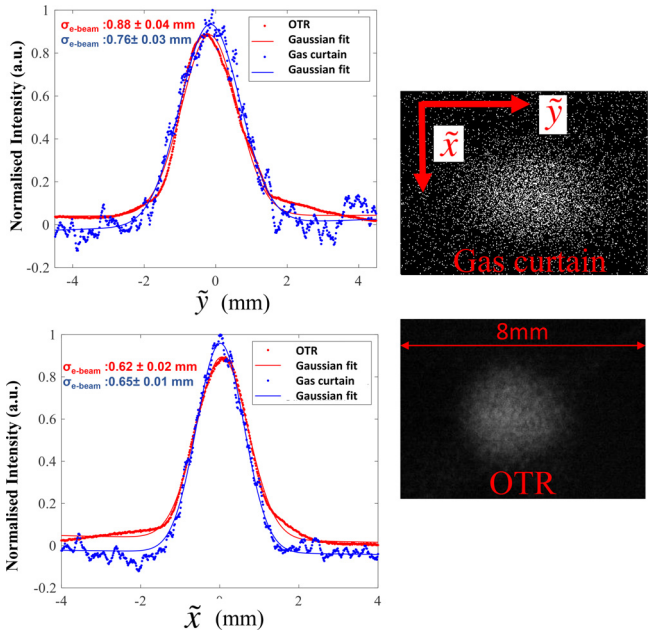

FIG. 4. Horizontal and vertical profiles of the CI electron beam (5 keV) imaged using a gas curtain and an OTR screen (normalized to the highest peak). For the gas curtain measurements, the integration time was set to 400 s.

Profile distortion due to the space charge and external electromagnetic fields can be pronounced for charged emitters such as nitrogen and argon. For the monitor deployed at the CI, these effects can be ignored. For the monitor to be installed at the LHC, the fluorescence image of the proton beam under the effects of the space charge and the magnetic fields present were simulated using IPMsim.[52] For the ionic nitrogen emitter (N_2^+ at 391.4 nm), although it has a higher cross section and thus short integration time, the measured beam size will increase from 0.35 to 0.49 mm under the space charge influence of a single bunch beam and 0.57 mm for a bunch train spaced 25 ns. However, the effect can be eliminated by using a neutral emitter such as neon at 585 nm.

Figure 5 shows a comparison of $\tilde{x}$ profiles obtained of the electron beam using nitrogen, neon, and argon gas curtains, respectively. The RMS size of the beam in the $\tilde{x}$ direction was measured to be 0.70 ± 0.08 and 0.62 ± 0.06 mm for argon and neon, respectively. For the profiles shown, both the background and residual gas signal have been subtracted from the gas curtain signal. The integration time was 400 s for nitrogen and 4000 s for neon and argon, which was chosen to show a good two-dimensional profile and improve the S/N ratio for the photon rate measurements. The higher integration time for neon and argon is due to their lower fluorescence cross sections and, in the case of neon, also lower detection efficiency. Furthermore, it is also due to the higher background stray light of the thermal electron gun source, which also emits light with a peak in the wavelength range where argon and neon have strong fluorescence lines. For an environment such as the LHC, this source is not a concern, but stray light due to the synchrotron radiation could be. Therefore, a low reflectivity coating, such as Multilayer sputtering (99.7% absorption) and Vantablack (99.965% absorption), are considered for future applications to reduce the background contribution and thus increase the S/N ratio.

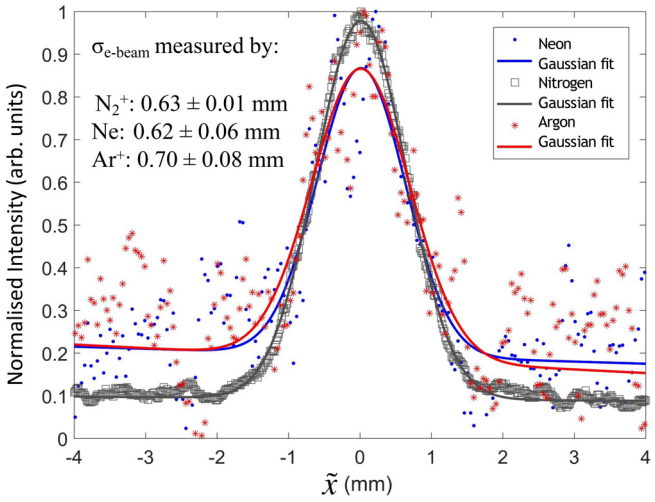

FIG. 5. The vertical profile of the CI electron beam (5 keV) measured by nitrogen, argon, and neon gas curtains (normalized to the highest peak). For nitrogen the integration time was set to 400 s, for neon and argon the integration time was increased to 4000 s.

In Fig. 5, the profiles measured from the three working gases show that the beam centroid aligns well, which confirms that the same source is measured. The RMS size measured from each gas curtain matches very well even though there are higher statistical errors for neon and argon and a lower S/N ratio.

The photon rate can be inferred from the acquired data; this was measured to be 18.0 ± 0.3, 1.2 ± 0.1, and 1.2 ± 0.1 photons/s for nitrogen, argon, and neon, respectively. The error here only includes a fitting error. The real error for the photon rate measurement could include the miscounting of the dark and stray photons which are not uniformly generated and the under counting of the signal photons which are below the detecting threshold. Nevertheless, experimental photon rates are within the error range of those presented in Table II, and therefore, the estimated photon rates in Table II can be expected in future HEL and LHC measurements. Since the estimated photon rates are much higher for the subsequent cases, the expected integration time will be greatly reduced. For neon, the potential working gas for monitors deployed at the LHC, one can expect an integration time of the order of 1 s for measuring the relative position of the proton beam with respect to the hollow electron beam.

In this Letter, a BIF based two-dimensional beam profile monitor utilizing a supersonic gas curtain has been presented. The transverse profile of an electron beam was measured from the fluorescence generated at various wavelengths from neon, argon, and nitrogen gas curtains. The measured signal intensity for each gas is in agreement with the estimated cross sections and experimental conditions for an electron beam at 5 keV. Furthermore, the agreement with the profiles assessed using an OTR method strengthens our confidence in these measurements.

This monitor is operable and compatible with UHV conditions as the pressure in the interaction chamber did not exceed 5×10^{-9} mbar, even with the gas curtain flowing through the system. Moreover, the profile measurements using neon demonstrate the feasibility of deploying such a monitor at the LHC/HEL as neon is one of the acceptable gases to be injected into the LHC vacuum system. For neon, no image

distortions will be seen from space charge and external electromagnetic fields. Furthermore, given the increase in beam intensity compared to the laboratory electron beam, the integration time can be reduced to seconds. Likewise, this monitor can be tailored as a noninvasive imaging system for profile measurement for other high intensity accelerators, either electrons or hadrons facilities, where other techniques do not exist.

Recently, two monitors based on the principle presented here were built under the Beam gas curtain (BGC) collaboration and are intended to be installed for the HEL test stand and the LHC. Future developments will focus on the design of a minimally invasive continuous overlap monitor for the primary proton beam and the surrounding hollow electron beam to be integrated into the HEL with potential profile monitoring capabilities. The future designs are more compact to address the geometrical constraints. This has the additional benefit of increasing the gas curtain density, due to the reduced distance between the nozzle and interaction chamber. Thus, a further reduction in integration times can be expected.

This work was supported by the HL-LHC project (CERN-UK collaboration) and by the Science and Technology Facilities Council (STFC), United Kingdom under the HL-LHC-UK phase II project ST/T001925/1 and the Cockcroft Institute core grant ST/G008248/1.

AUTHOR DECLARATIONS

Conflict of Interest

The authors have no conflicts to disclose.

DATA AVAILABILITY

The data that support the finding of this study are available within the article and the raw data of this study are available from the corresponding author upon reasonable request.

REFERENCES

[1]O. Aberle, I. Béjar Alonso, O. Brüning *et al.*, "High-luminosity Large Hadron Collider (HL-LHC): Technical design report," Report No. CERN-2020-010 (2020).
[2]V. Shiltsev, Y. Alexahin, K. Bishofberger, V. Kamerdzhiev, G. Kuznetsov, and X.-L. Zhang, "Experimental demonstration of colliding-beam-lifetime improvement by electron lenses," Phys. Rev. Lett. **99**, 244801 (2007).
[3]G. Stancari, A. Valishev, G. Annala, G. Kuznetsov, V. Shiltsev, D. A. Still, and L. G. Vorobiev, "Collimation with hollow electron beams," Phys. Rev. Lett. **107**, 084802 (2011).
[4]X. Gu, W. Fischer, Z. Altinbas, A. Drees, J. Hock, R. Hulsart, C. Liu, A. Marusic, T. A. Miller, M. Minty, G. Robert-Demolaize, Y. Tan, P. Thieberger, H. G. Morales, D. Mirarchi, S. Redaelli, A. I. Pikin, and G. Stancari, "Halo removal experiments with hollow electron lens in the BNL relativistic heavy ion collider," Phys. Rev. Accel. Beams **23**, 031001 (2020).
[5]M. Fitterer, G. Stancari, A. Valishev, S. Redaelli, and D. Valuch, "Resonant and random excitations on the proton beam in the Large Hadron Collider for active halo control with pulsed hollow electron lenses," Phys. Rev. Accel. Beams **24**, 021001 (2021).
[6]S. Redaelli, R. Appleby, R. Bruce, O. Brüning, A. Kolehmainen, G. Ferlin, A. Foussat, M. Giovannozzi, P. Hermes, D. Mirarchi, D. Perini, A. Rossi, and G. Stancari, "Hollow electron lenses for beam collimation at the High-luninosity Large Hadron Collider (HL-LHC)," J. Instrum. **16**, P03042 (2021).
[7]R. Anne, Y. Georget, R. Hue, C. Tribouillard, and J. L. Vignet, "A noninterceptive heavy ion beam profile monitor based on residual gas ionization," Nucl. Instrum. Methods Phys. Res., Sect. A **329**, 21–28 (1993).
[8]J. Mießner, M. Sachwitz, M. Markert, R. Sternberger, K. Tiedtke, and A. Hofmann, "An ionization profile monitor for the determination of the flash photon beam parameter," Nucl. Instrum. Methods Phys. Res., Sect. A **635**, S104–S107 (2011).
[9]D. Bartkoski, C. Deibele, and Y. Polsky, "Design of an ionization profile monitor for the SNS accumulator ring," Nucl. Instrum. Methods Phys. Res., Sect. A **767**, 379–384 (2014).
[10]H. S. Sandberg, W. Bertsche, D. Bodart, S. Gibson, S. Levasseur, K. Satou, G. Schneider, J. W. Storey, and R. Veness, "Measuring the beam profile by counting ionization electrons," in *Proceedings 8th International Beam Instrumentation Conference (IBIC'19)* (JACoW Publishing, 2019), pp. 257–260.
[11]H. S. Sandberg, W. Bertsche, D. Bodart, S. Jensen, S. Gibson, S. Levasseur, K. Satou, G. Schneider, J. W. Storey, and R. Veness, "Commissioning of timepix3 based beam gas ionisation profile monitors for the CERN proton synchrotron," in *9th International Beam Instrumentation Conference (IBIC'21)* (JACoW Publishing, 2021), p. 172.
[12]A. Variola, R. Jung, and G. Ferioli, "Characterization of a nondestructive beam profile monitor using luminescent emission," Phys. Rev. ST Accel. Beams **10**, 122801 (2007).
[13]T. Tsang, D. Gassner, and M. Minty, "Residual gas fluorescence monitor for relativistic heavy ions at RHIC," Phys. Rev. ST Accel. Beams **16**, 102802 (2013).
[14]P. Forck and A. Bank, "Residual gas fluorescence for profile measurements at the GSI UNILAC," in Proceedings of the 6th European Workshop on Beam Diagnostics and Instrumentation for Particle Accelerators, 2002.
[15]P. Forck, "Minimal invasive beam profile monitors for high intense hadron beams," in *Proceedings of 1st International Particle Accelerator Conference (IPAC'10)* (Kyoto, Japan, 2010) pp. 1261–1265.
[16]F. Becker, C. Andre, P. Forck, and D. Hoffmann, "Beam induced fluorescence (BIF) monitor for transverse profile determination of 5 to 750 MeV/u heavy ion beams," in 8th European Workshop on Beam Diagnostics and Instrumentation for Particle Accelerators (DIPAC), 2007.
[17]A. Alexopoulos, C. Barschel, E. Bravin, G. Bregliozzi, N. Chritin, B. Dehning, M. Ferro-Luzzi, M. Giovannozzi, R. Jacobsson, L. Jensen, R. Jones, V. Kain, R. Kieffer, R. Matev, M. Rihl, V. S. Guimaraes, R. Veness, S. Vlachos, B. Würkner, A. Bay, F. Blanc, S. Giani, O. Girard, G. Haefeli, P. Hopchev, A. Kuonen, T. Nakada, O. Schneider, M. Tobin, Z. Xu, R. Greim, T. Kirn, S. Schael, M. Wlochal, and BGV Collaboration, "Noninvasive LHC transverse beam size measurement using inelastic beam-gas interactions," Phys. Rev. Accel. Beams **22**, 042801 (2019).
[18]B. Vosicki and K. Zankel, "The sodium curtain beam profile monitor of the ISR," IEEE Trans. Nucl. Sci. **22**, 1475–1478 (1975).
[19]A. V. Bubley, V. I. Kudelainen, V. V. Parkhomchuk, B. M. Smirnov, and V. S. Tupikov, "Magnesium jet profile monitor," in *Proceedings of the 17th International Conference on High-Energy Accelerators* (Dubna, Russia, 1998), p. 357–359.
[20]T. Tsang, S. Bellavia, R. Connolly, D. Gassner, Y. Makdisi, T. Russo, P. Thieberger, D. Trbojevic, and A. Zelenski, "Optical beam profile monitor and residual gas fluorescence at the relativistic heavy ion collider polarized hydrogen jet," Rev. Sci. Instrum. **79**, 105103 (2008).
[21]V. Tzoganis and C. P. Welsch, "A non-invasive beam profile monitor for charged particle beams," Appl. Phys. Lett. **104**, 204104 (2014).
[22]V. Tzoganis, H. D. Zhang, A. Jeff, and C. P. Welsch, "Design and first operation of a supersonic gas jet based beam profile monitor," Phys. Rev. Accel. Beams **20**, 062801 (2017).
[23]Y. Hashimoto, T. Fujisawa, T. Morimoto, Y. Fujita, T. Honma, S. Muto, K. Noda, Y. Sato, and S. Yamada, "Oxygen gas-sheet beam profile monitor for the synchrotron and storage ring," Nucl. Instrum. Methods Phys. Res., Sect. A **527**, 289–300 (2004).
[24]T. Fujisawa, Y. Hashimoto, T. Morimoto, and Y. Fujita, "Multi-pole magnets to focus an O_2 sheet beam for a non-destructive beam-profile monitor," Nucl. Instrum. Methods Phys. Res., Sect. A **506**, 50–59 (2003).
[25]V. Shiltsev, "Space-charge effects in ionization beam profile monitors," Nucl. Instrum. Methods Phys. Res., Sect. A **986**, 164744 (2021).
[26]I. Yamada, M. Wada, K. Moriya, J. Kamiya, P. K. Saha, and M. Kinsho, "High-intensity beam profile measurement using a gas sheet monitor by beam induced fluorescence detection," Phys. Rev. Accel. Beams **24**, 042801 (2021).

[27]K. Chipps, U. Greife, D. Bardayan, J. Blackmon, A. Kontos, L. Linhardt, M. Matos, S. Pain, S. Pittman, A. Sachs, H. Schatz, K. Schmitt, and M. Smith, "The jet experiments in nuclear structure and astrophysics (JENSA) gas jet target," Nucl. Instrum. Methods Phys. Res., Sect. A **763**, 553–564 (2014).
[28]A. Kontos, D. Schürmann, C. Akers, M. Couder, J. Görres, D. Robertson, E. Stech, R. Talwar, and M. Wiescher, "Hippo: A supersonic helium jet gas target for nuclear astrophysics," Nucl. Instrum. Methods Phys. Res., Sect. A **664**, 272–281 (2012).
[29]J. Couperus, A. Köhler, T. Wolterink, A. Jochmann, O. Zarini, H. Bastiaens, K. Boller, A. Irman, and U. Schramm, "Tomographic characterisation of gas-jet targets for laser wakefield acceleration," Nucl. Instrum. Methods Phys. Res., Sect. A **830**, 504–509 (2016).
[30]G. Stancari, V. Previtali, A. Valishev, R. Bruce, S. Redaelli, A. Rossi, and B. S. Ferrando, "Conceptual design of hollow electron lenses for beam halo control in the Large Hadron Collider," Report No. CERN-ACC-2014-0248 (2014).
[31]J. Glutting, "Alignment of nozzle and skimmers at micron scale and support of the experimental setup for the beam gas curtain (BGC) instrument," Master's thesis (Engineering Dept. Hochschule Kaiserslautern, University of Applied Sciences, Kaiserslautern, Germany, 2018).
[32]G. Scoles, *Atomic and Molecular Beam Methods* (Oxford University Press, 1998), Vol. 1, pp. 14–30.
[33]H. D. Zhang, A. Salehilashkajani, C. P. Welsch, M. Ady, J. Glutting, O. R. Jones, T. Marriott-Dodington, S. Mazzoni, A. Rossi, G. Schneider, R. Veness, P. Forck, and S. Udrea, "Development of supersonic gas-sheet-based beam profile monitors," in *Proceedings of 10th International Particle Accelerator Conference (IPAC'19), Melbourne, Australia, 19–24 May 2019* (JACoW Publishing, Geneva, Switzerland, 2019), pp. 2717–2720.
[34]S. Udrea, P. Forck, E. B. Diaz, N. Chritin, O. R. Jones, P. Magagnin, G. Schneider, R. Veness, V. Tzoganis, C. Welsch, and H. Zhang, "Development of a fluorescence based gas sheet profile monitor for use with electron lenses: Optical system design and preparatory experiments," in *Proceedings of International Beam Instrumentation Conference (IBIC'17), Grand Rapids, MI, 20–24 August 2017* (JACoW, Geneva, Switzerland, 2018), pp. 359–363.
[35]L. Hirvonen, M. Barber, and K. Suhling, "Photon counting imaging and centroiding with an electron-bombarded CCD using single molecule localisation software," Nucl. Instrum. Methods Phys. Res., Sect. A **820**, 121–125 (2016).
[36]L. Hirvonen, F. Festy, and K. Suhling, "Wide-field time-correlated single-photon counting (TCSPC) lifetime microscopy with microsecond time resolution," Opt. Lett. **39**, 5602–5605 (2014).
[37]S. Udrea and P. Forck, "Milestone 1.1 and 1.6 report," Report No. CERN-EDMS-2333411 and CERN-EDMS-2333413 (2018).
[38]R. Veness, M. Ady, N. S. Chritin, J. Glutting, T. Marriott-Dodington, O. R. Jones, R. Kersevan, S. Mazzoni, A. Rossi, G. Schneider, P. Forck, S. Udrea, A. Salehilashkajani, C. P. Welsch, and H. D. Zhang, "Development of a beam-gas curtain profile monitor for the high luminosity upgrade of the LHC," in *Proceedings of 7th International Beam Instrumentation Conference (IBIC'18), Shanghai, China, 09–13 September 2018* (JACoW Publishing, Geneva, Switzerland, 2019), pp. 472–476.
[39]W. L. Borst and E. C. Zipf, "Cross section for electron-impact excitation of the (0,0) first negative band of N_2^+ from threshold to 3 keV," Phys. Rev. A **1**, 834–840 (1970).
[40]V. Puech and S. Mizzi, "Collision cross sections and transport parameters in neon and xenon," J. Phys. D **24**, 1974–1985 (1991).
[41]J. Bretagne, G. Callede, M. Legentil, and V. Puech, "Relativistic electron-beam-produced plasmas. I. Collision cross sections and loss function in argon," J. Phys. D **19**, 761–777 (1986).
[42]M. Plum, E. Bravin, J. Bosser, and R. Maccaferri, "N_2 and Xe gas scintillation cross-section, spectrum, and lifetime measurements from 50 MeV to 25 GeV at the CERN PS and booster," Nucl. Instrum. Methods Phys. Res., Sect. A **492**, 74–90 (2002).
[43]M. Eckhardt, D. Hasselkamp, and K. H. Schartner, "Neon 3*p*-excitation by proton impact (100 keV–1 MeV): Cross sections and line polarization," Z. Phys. A **292**, 337–345 (1979).
[44]Y. Itikawa, "Cross sections for electron collisions with nitrogen molecules," J. Phys. Chem. Ref. Data **35**, 31–53 (2006).
[45]D. E. Shemansky, J. M. Ajello, and I. Kanik, "Electron excitation function of the N_2 second positive system," Astrophys. J. **452**, 472 (1995).
[46]D. F. Register, S. Trajmar, G. Steffensen, and D. C. Cartwright, "Electron-impact-excitation cross sections for electronic levels in neon for incident energies between 25 and 100 eV," Phys. Rev. A **29**, 1793–1810 (1984).
[47]F. A. Sharpton, R. M. St. John, C. C. Lin, and F. E. Fajen, "Experimental and theoretical studies of electron-impact excitation of neon," Phys. Rev. A **2**, 1305–1322 (1970).
[48]J. B. Boffard, B. Chiaro, T. Weber, and C. C. Lin, "Electron-impact excitation of argon: Optical emission cross sections in the range of 300–2500 nm," At. Data Nucl. Data Tables **93**, 831–863 (2007).
[49]S. Tsurubuchi, "Emission cross sections of Ar^+ measured in a wide range of electron impact energies," J. Phys. Soc. Jpn. **66**, 3070–3073 (1997).
[50]I. D. Latimer and R. M. S. John, "Simultaneous excitation and ionization of argon by electrons to the upper laser states of Ar^+," Phys. Rev. A **1**, 1612–1615 (1970).
[51]A. Kramida, Y. Ralchenko, J. Reader, NIST ASD Team *et al.*, https://physics.nist.gov/asd for "NIST Atomic Spectra Database (ver. 5.8)," National Institute of Standards and Technology, Gaithersburg, MD, 2020.
[52]D. Vilsmeier, M. Sapinski, R. Singh, and J. Storey, "Reconstructing space-charge distorted IPM profiles with machine learning algorithms," J. Phys.: Conf. Ser. **1067**, 072003 (2018).